1-1-2012

Contact pressure distribution of osteochondral defects of the knee: effects of non-vertical walls

Scott Ensminger
Wayne State University,

CONTACT PRESSURE DISTRIBUTION OF OSTEOCHONDRAL DEFECTS OF THE KNEE: EFFECTS OF NON-VERTICAL WALLS

by

SCOTT ENSMINGER

THESIS

Submitted to the Graduate School

of Wayne State University,

Detroit, Michigan

in partial fulfillment of the requirements

for the degree of

MASTER OF SCIENCE

2012

MAJOR: MECHANICAL ENGINEERING

Approved by:

_____

Advisor Date

ACKNOWLEDGEMENTS

The author would like to thank Mamtha Balasubramaniam, the staff biostatistician at the William Beaumont Hospital Research Institute, for her completion of the statistical analysis of this data. Also the author would like to thank Dr. Constantine Demetropoulos, Dr. King Yang, Dr. Kathy Coyner, Dr. Joseph Guettler, Dr. Kenneth Jurist, Kevin Baker and Dana Vanderlaan for their continued help and support in this endeavor**.**

Before the publication of this thesis, some findings of this research were submitted for publication in the Journal of Arthroscopy. As of this writing the submission has yet to be approved by the Journal of Arthroscopy.

TABLE OF CONTENTS

LIST OF TABLES

LIST OF FIGURES

INTRODUCTION

Historical Background

Articular cartilage is a substance with mechanical properties that has not been reproduced by any synthetic material. It is durable, resists impact, resists wear, has low friction and can bear millions of cycles of heavy loading and unloading. For many joints the articular cartilage will last a lifetime without any signs of wear. By all accounts, articular cartilage is quite extraordinary. Because of its many qualities it is an integral part of normal joint motion.

However, defects in the cartilage can cause pain and may lead to the onset of further damage to the surrounding cartilage. In adults, articular cartilage has a limited capacity to heal, leaving physicians with difficult choices to make regarding repair[14]. Physicians commonly recommend one of several accepted cartilage restoration therapies to repair the damaged cartilage. However, choosing which cartilage therapy to perform can be a difficult task as outcomes vary based on many factors including the severity of the lesion, the chosen procedure and the patient's age, height, weight, activity level, symptoms and comorbidities[15]. Determining the need for surgical intervention based on these factors is not well understood. A literature review demonstrated a paucity of empirical studies to investigate these factors. Brown et al. and Guettler et al. explored osteochondral lesions as a factor by finding a link between full thickness well-shouldered defects and contact stresses in the surrounding cartilage in canine and cadaveric models[2,10], respectively. Guettler et al.[10] research concluded that defects of a diameter of 10 mm or more alter contact stress concentrations, and may be a useful adjunct to guide clinical decision making.

Based on their findings, this report proposes an empirical investigation of how lesion geometry may further affect contact stress concentrations in the adjacent cartilage, as most clinically observed lesions are not well-shouldered[5]. This study will explore how lesions with a beveled border (more naturally occurring) compare with the well-shouldered lesions studied previously. It will also determine if there is a correlation between said lesions and contact stress concentrations on the adjacent cartilage. Our hope is to determine a size and shape guideline for physicians to use when determining if surgical intervention is necessary.

Biomechanics of Articular Cartilage

It is important to understand the makeup and physical behavior of articular cartilage. Mechanically, articular cartilage may be considered metaphorically. Two simple objects to compare it with are a sponge and an air cushion, both of which the cartilage shares various characteristics. Like a sponge, articular cartilage will compress quickly under loading, but take some time to revert to its pre-deformed geometry. This is due to the fact that healthy cartilage is made up of almost 80% water[8]. Yet unlike a sponge and more like an air cushion, articular cartilage has a tough outer layer that protects the cartilage and underlying subchondral bone. This outer surface also acts as a low friction bearing surface. These properties can be further understood by understanding the microstructure of articular cartilage.

A simple way to conceptualize articular cartilage and its microstructure is to consider it layer by layer. The superficial layer (articular surface) of the cartilage is called the lamina splendens and has been referred to as the armored plate layer[1]. It is

composed of collagen fibers and elongated chondrocytes, both in parallel alignment with the articular surface. This dense area of aligned collagen fibers creates the metaphorical outer pocket that both protects the cartilage and creates an exceptional bearing surface. The physical orientation of the collagen fibers is what gives this surface its characteristics. Tightly packed and aligned fibers leave only very small pores for fluids to enter and exit[8]. The alignment orthogonal to the typical direction of loading allows for the load to be mostly supported by the structures below. This alignment also creates strength in the transverse direction protecting against tears caused by loading in an atypical orientation.

The middle and deep regions are also made up of chondrocytes and collagen fibers. In contrast with the top layer, the middle region has a lower density of collagen fibers that are not all oriented parallel to the articular surface. The chondrocytes are larger and rounder in this region.

The deep region is similar to the middle region except that the collagen fibers in this region are found to be aligned orthogonal to the articular surface. Also, the chondrocytes in this region are aligned vertically in rows. The vertically aligned collagen fibers help to keep the cartilage from tearing away from the calcified zone and subchondral bone.

Finally the lower layer of the cartilage is called the calcified zone and is separated from the deep region by the tidemark. This layer is a transitional layer that anchors the overlying cartilage to the subchondral bone.

Figure 1 shows the tissue structure of articular cartilage. As explained, the collagen fibers and chondrocytes most superficial are aligned parallel to the articular surface. Lower in the joint the fibers and chondrocytes progressively orient more

orthogonal to the articular surface. Finally the lowest level is the calcified zone and is separated from the upper layers.

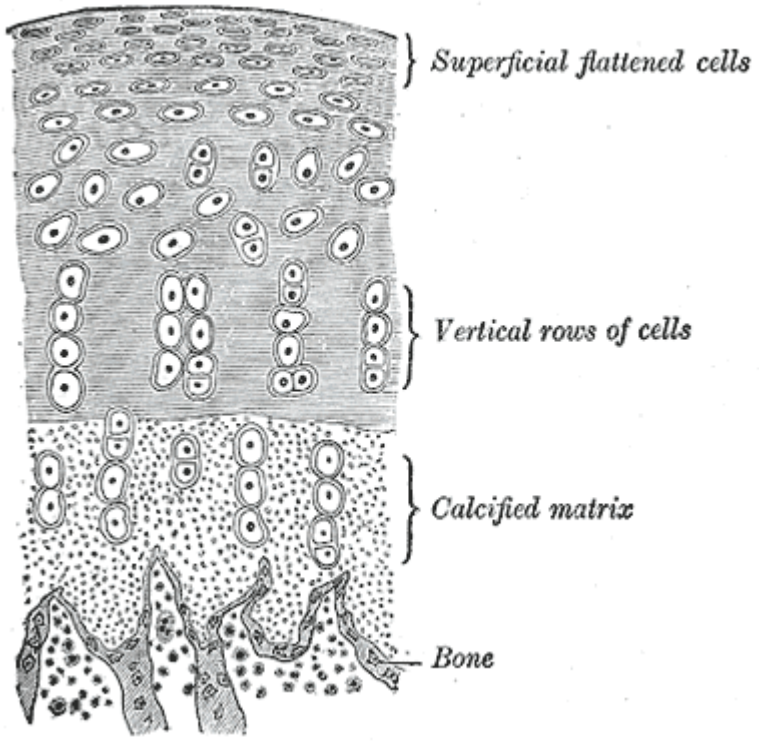

Figure 1.[9] Tissue structure of articular cartilage.

In understanding the macroscopic and mechanical properties of articular cartilage we must also understand its microscopic composition as a composite material. At the microscopic level, articular cartilage is made up of chondrocytes surrounded by an extracellular matrix. This matrix is made up of water, proteoglycan, collagen, and various other proteins and glycoproteins[8]. Unlike other biological materials, articular cartilage contains no blood vessels, lymphatics or nerves, to which its inability to heal may be attributed[8]. The makeup of the extracellular matrix plays an important role in the joint biomechanics. The 65-80% water weight normally present in articular cartilage is very important in handling compressive loads across the joint. The small pores present in the extracellular matrix make it difficult for a large molecule such as water to pass

through. Therefore, there is a good amount of frictional resistance to the water leaving the matrix as the cartilage is compressed. Also, due to the relative incompressibility of water coupled with the inability of these large molecules to easily leave the matrix, the cartilage is able to support very heavy loads.

Another material that has a significant impact on the biomechanics of the cartilage is collagen. Collagen makes up about 60% of the dry weight of articular cartilage[8]. As described before, collagen fibers are located throughout the depth of articular cartilage. These fibers are oriented parallel to the surface in areas close to the surface and orthogonal to the surface in deeper areas. Like inorganic fiber reinforced materials, these organic fibers give the cartilage its tensile strength.

Articular cartilage is a biphasic material consisting of a solid phase and a fluid phase. The solid phase is responsible for the tensile strength of the material. The fluid phase is responsible for ability of the material to resist deformation and carry compressive loads up to 20 times body weight during jumping[8]. In fact in normal loading of healthy cartilage, interstitial fluid supports more than 95% of the total applied load[8,19].

It is also important to note the viscoelasticity of articular cartilage. Viscoelastic behavior describes a material whose strain-rate is time dependent. What this means is a viscoelastic material loses energy when a load is applied, then removed. Hysteresis is observed in the stress-strain curve, with the area of the loop being equal to the energy lost during the loading cycle. In articular cartilage, this behavior is caused by two factors; the fluid flow in and out of the pores and its resulting frictional drag (or the inverse of the permeability of the solid phase), and the intermolecular friction of its proteoglycan matrix.

Defects in articular cartilage have been found to have many causes. Osteoarthritis typically leads to lesions in the articular cartilage with tricompartmental disease, typically showing deterioration of the cartilage. Also patients with a genetic predisposition to the development of degenerative arthritis are commonly found to show degeneration in all three compartments of the knee[5]. Cartilage defects can also be caused by trauma leading to the onset of osteoarthritis[21].

Understanding

Based on the complex physical structure and inability to heal itself, a common topic discussed in the literature[5,15] is how to choose the correct restoration therapy based on the identified cartilage defect. Restoration therapies in general include allografts and autografts of existing healthy cartilage, microfracture and other treatments that place healthy cartilage at the site of a lesion, or promote repair. Recent studies have determined that allograft and autograft treatments result in the best patient outcomes in 5 and 10 year follow up studies of pain, range of motion and other metrics of joint function[5]. However, due to the invasive nature of these treatments the physician is left to ask which defects should be treated and which should be left alone. There are many differing opinions on what types of articular cartilage defects can constitute treatable defects. This question was first answered in two studies that utilized canine[2] and cadaveric[10] specimens. These studies revealed that defect size does have a marked effect on pressure distributions in surrounding cartilage where a larger size defect redistributes the contact pressures to further outlying areas of the cartilage, which the authors postulate may promote further degeneration. The authors also believe that there is a minimum defect size of 10 mm[10] which physicians can use as a guide in determining whether to

treat lesions in weight bearing areas of the knee. In these studies defect geometry was not a tested variable and only cylindrical "well-shouldered" defects were created. However, in practice articular cartilage defects can have differing geometries. Some may be similar to the cylindrical defects examined in previous studies, but clinical experience shows that defects will most often have longer sloping edges and may not be circular at all. This study aims to examine the relationship between the well-shouldered defects studied previously, and compares and contrasts them with defects of different geometries. Comparing the odd shaped (beveled) defects with those studied previously will help physicians to better understand defects based on both size and geometry and better predict how patient prognoses are affected.

METHODS

Ten fresh-frozen cadaveric knee specimens were used for this study. These specimens consisted of five left knees and five right knees from five cadavers. Each cadaver was selected taking care that it had no history or indications of cartilage damage or joint pathology. After specimens were acquired, each was examined pre-dissection using radiography to screen for joint malalignment and arthritis. Specimens ranged in age from 64 to 69 years with the median age being 65 years. Female donors accounted for 60% of the specimens while male donors accounted for 40%.

Specimens were prepared for testing by removing all soft tissue superior and inferior to the joint capsule. The patella was removed and capsule resected taking special care to avoid causing any ligament damage. Fatty tissue anterior to the meniscus was removed to aid in proper instrument placement. Specimens were cleaned of any remaining soft tissue that may have hindered the potting process.

Following dissection both ends of each specimen were carefully potted in polyester resin. In potting, the knee was positioned with the femoral and tibial diaphyses orthogonal to the potting surface. This positioning allowed the knee to be loaded in an anatomically appropriate orientation, while being fixed to a rigid testing apparatus. The material was allowed to sufficiently harden before testing.

Positioning of the knee was a critical variable that was controlled by multiple methods. As mentioned above, the knee was potted in a way that it sat orthogonal to the potting base. With all ligaments left intact the specimen was placed in a custom designed loading fixture. This fixture consisted of two jigs specially designed for the static loading of a knee. The portion of the fixture holding the tibia was a fixed rigid tube that held the

tibia in an axial alignment with the load frame actuator arm. The superior portion allowed for adjustment of the femoral condyles in translation and rotation. The fixture was adjusted so that each knee could be held at 30° of flexion, while still being constrained by the relevant anatomical structures. After proper placement was determined, the femur was rigidly locked into place and not moved until testing was completed. Following placement ligaments crossing the joint line were sectioned allowing sensors to be easily placed in the medial and lateral compartments above the meniscus. This also allowed access to the knee joint such the defects would be accurately created in subsequent steps of the protocol.

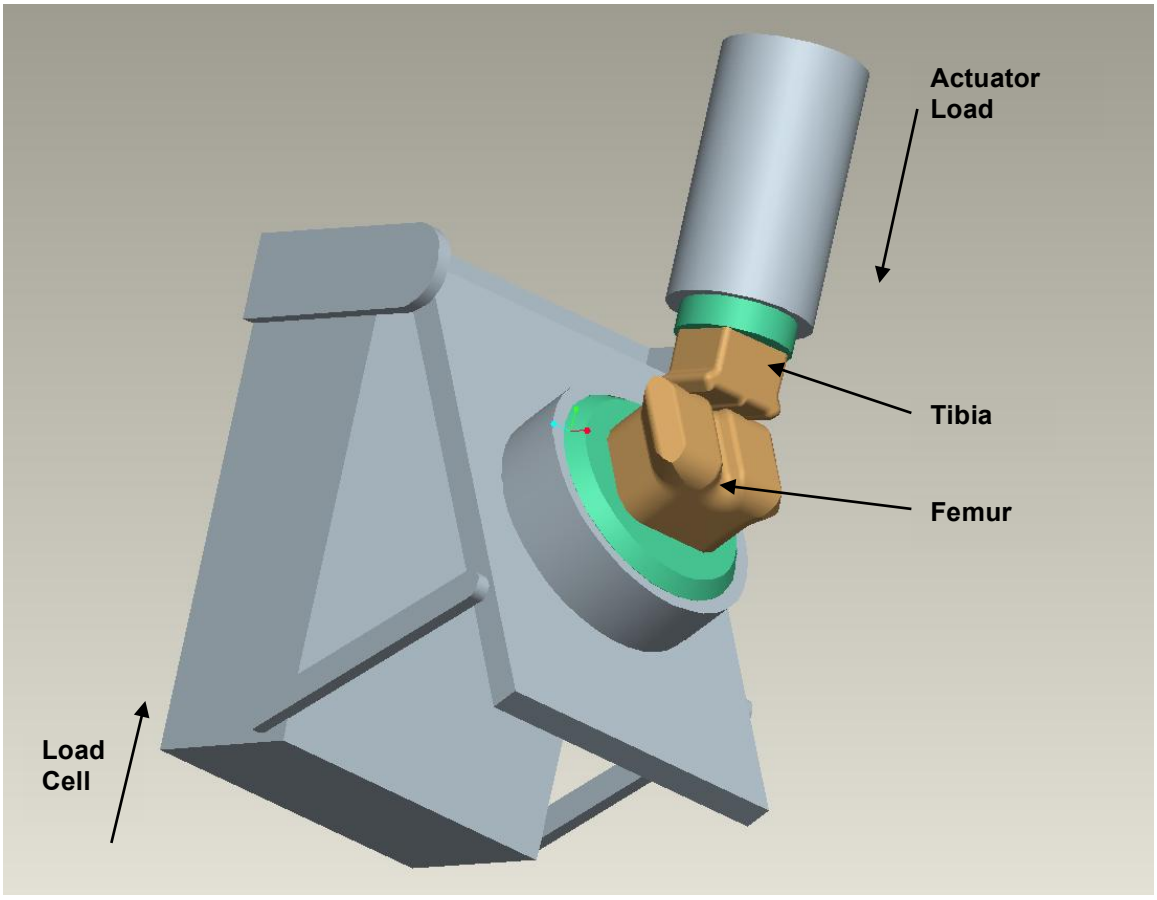

Figure 2. Experimental test set up diagram showing placement and directions of loading.

Paper-thin digital electronic pressure sensors (K-scan 4000, Tekscan, Boston, Mass) were used for *in situ* pressure measurement. Each of two sensor pads (one for each condyle) consists of a printed circuit of load sensing regions aligned in a grid measuring 28 mm X 33 mm. This grid contained 572 regions or sensels measuring 0.8 mm by 1.0 mm each. Prior to testing, the both sensor pads were equilibrated and calibrated. Equilibration consisted of placing the sensor pads in a uniform pressure bladder under constant pressures of 80psi, 90psi and 100psi in order to equalize sensitivity across the sensels. Pressure measurements were taken at each pressure to create a 3-point equilibration. Following equilibration, each sensor pad was placed in the load frame (Mini-Bionix 858, MTS, Eden Prairie, Minn) to be calibrated in order to relate sensor output to physical loads. To ensure even loading during calibration, sensor pads were held between two Delrin plates during loading. A loading profile was created ramping from 10 N to 800 N then back down to 10 N with mid-peaks at 200 N. Calibration points were taken at 200 N and 800 N to create a calibration curve for each sensor pad. Sensors were marked to identify medial or lateral placement to avoid possible errors in data collection. Each sensor was also identified by number to allow changing of sensors during the testing process without mismatching calibration data. During insertion, care was taken not to crinkle the sensors as to avoid damaging the sensor or the underlying cartilage. As K-scan sensors have been known to measure inaccurately when encountering shear stresses, placing the knee in 30° of flexion helped to ensure a majority of contact stresses at the point of contact were compressive. This was due to the point of contact being over the flatter crown portion of the femoral condyles.

Each specimen load sensor was zeroed prior to any contact in the joint. Each knee was then loaded to 100 N with the sensors having already in place. Once 100 N was reached, fine adjustments were made to sensor placement in order to assure that the articular pressure distribution was well centered within the active pressure sensing region of the sensor pads. Loading was ramped from 100 N to 700 N at a rate of 100 N/s. The load was held at 700 N for 5 seconds and then ramped back down to 100 N and held again for 5 seconds. A peak load of 700 N was chosen in accordance with the previous study by Guettler et al.[10]. Dynamic pressure measurements were taken during the complete loading and unloading cycle. Only peak pressure values were used for analysis.

With the knee still under 100 N load, notice was taken of the approximate pressure distribution center. This position was then used as a guide for placement of a center mark for defect creation in the sagittal plane. In the coronal plane center position was established as half the condylar width, this combined center position was physically marked on the specimen as a reference for defect placement. The specimen was then unloaded completely and sensors were removed. Using the marked center, a cylindrical defect was created in each condyle using an osteochondral coring device (OATS, Arthrex, Naples, Florida). A core of 6 mm diameter and 12 mm depth was removed from the loading center of each the medial and lateral condyle. The sensor was again placed in the joint and a 100 N load was applied. Sensor position was adjusted with care taken to approximate the same positioning as used during the previous loading cycle. The same loading profile was used as previously mentioned and all data were recorded.

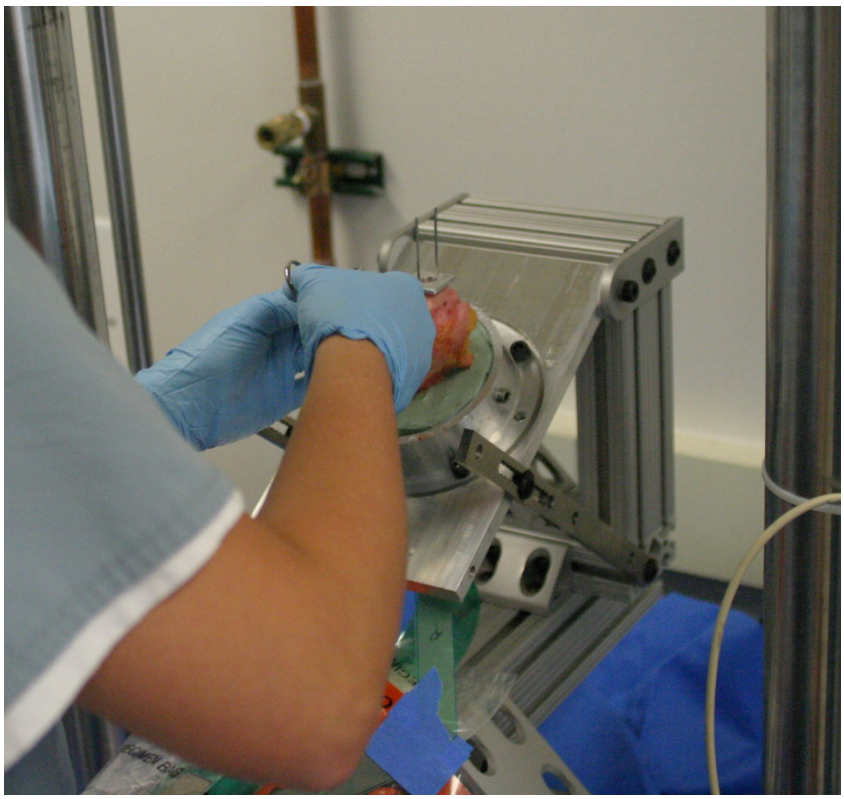

Figure 3. Specimen in jig during defect creation.

Figure 4. Specimen showing artificially created well-shouldered defect.

Following a second unloading and removal of the sensors a beveled edge was added to each defect. Specially designed guides were used along with a standard 82° woodworking countersink to create this bevel. The guide was placed concentric to the cylindrical defect and the countersink placed inside. The guide held the countersink on center, while allowing the cutting edge to only traverse 2 mm into the surface of the cartilage. This depth was predefined as a standard depth for all bevels so as not to reach the subchondral bone. After the beveled edges were added, the specimen was again loaded in the same manner as before, and all pressure data were collected. This process of creating cylindrical defects and then beveling the edges was repeated for defect sizes 6, 8, 10, 12, 14, 16, 18 and 20 mm. Specimens were constantly hydrated using normal saline and allowed a mimimum 15 minutes of rest between load cycles.

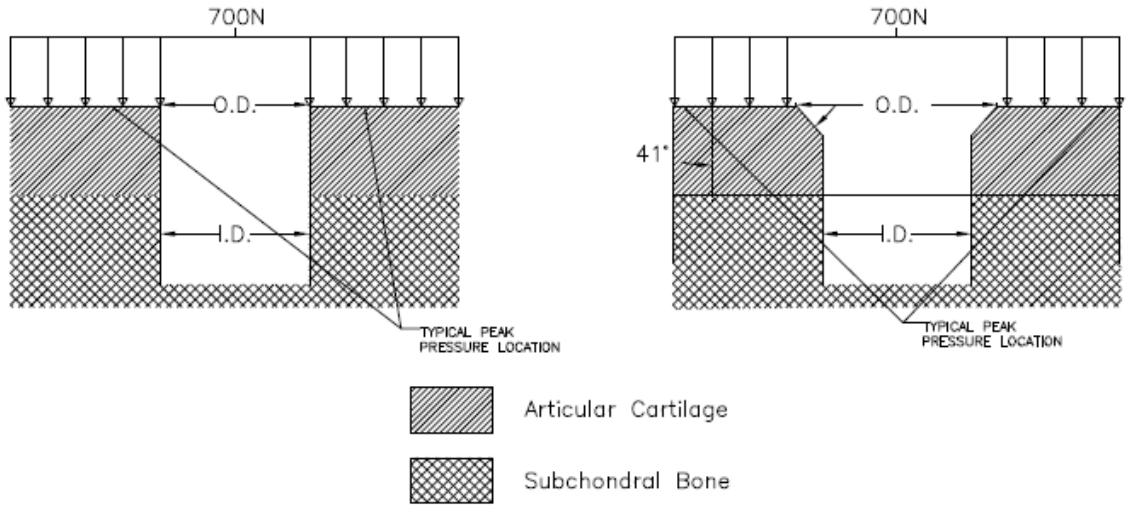

Figure 5. Shape and load distribution of well-shouldered defects (left) and beveled defects (right).

Figure 6. Specimen showing artificially created beveled defect.

Pressure distributions were digitally recorded for each test using the Tekscan digital acquisition software (ISCAN, Tekscan, South Boston, Mass). This software compiled the peak pressures from each sensel on the sensor pad over the full duration of the test. This information was displayed as a single image similar to that of previous Fuji Film methods. Each peak distribution was exported and the data characterized.

Characterization of the data consisted of manually determining the center of the defect (based on ISCAN readouts) and assigning a radius value to each pressure moving outwards concentrically. The outcome of this characterization gives a chart where each pressure value reading from the ISCAN is assigned a radius from center value. This conversion from a Cartesian grid to a polar coordinate grid created new opportunities for analysis and is analogous to the radial line method of analysis described by Brown et al.[2].

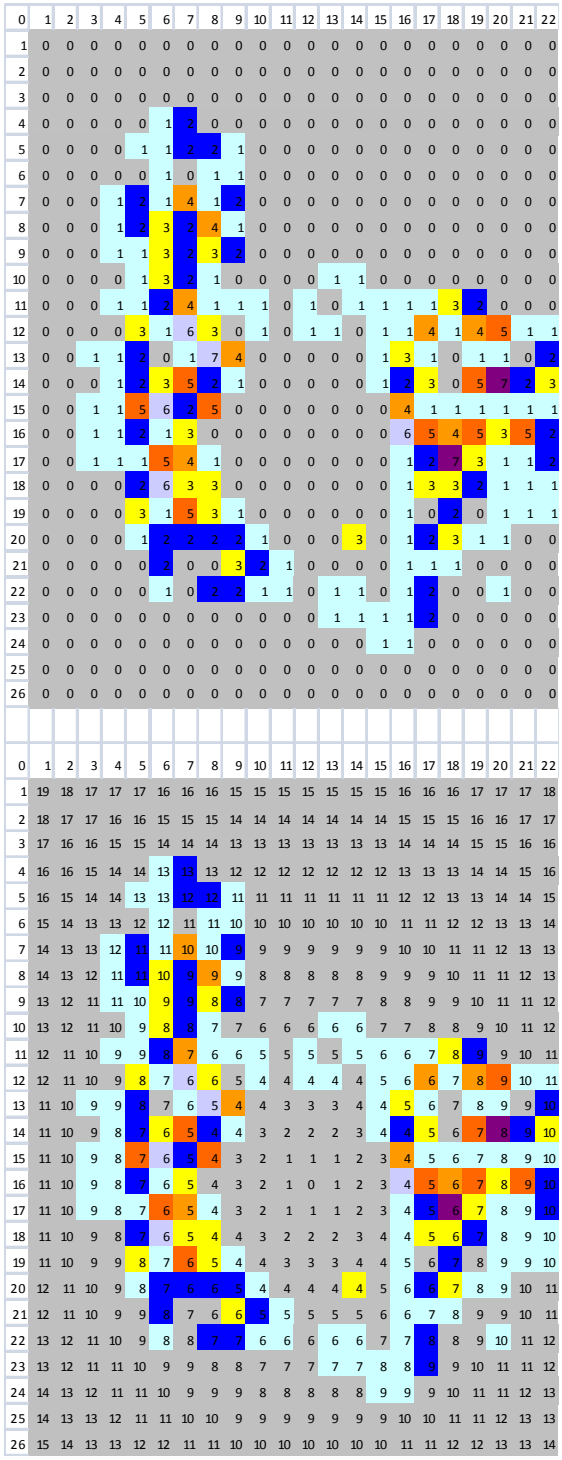

	0	1	2	3	4	5	6	7	8	9	10	11	12	13	14	15	16	17	18	19	20	21	22
1	0	0	0	0	0	0	0	0	0	0	0	0	0	0	0	0	0	0	0	0	0	0	0
2	0	0	0	0	0	0	0	0	0	0	0	0	0	0	0	0	0	0	0	0	0	0	0
3	0	0	0	0	0	0	0	0	0	0	0	0	0	0	0	0	0	0	0	0	0	0	0
4	0	0	0	0	0	0	1	2	0	0	0	0	0	0	0	0	0	0	0	0	0	0	0
5	0	0	0	0	0	1	1	2	2	1	0	0	0	0	0	0	0	0	0	0	0	0	0
6	0	0	0	0	0	0	1	0	1	1	0	0	0	0	0	0	0	0	0	0	0	0	0
7	0	0	0	0	1	2	1	4	1	2	0	0	0	0	0	0	0	0	0	0	0	0	0
8	0	0	0	0	1	2	3	2	4	1	0	0	0	0	0	0	0	0	0	0	0	0	0
9	0	0	0	0	1	1	3	2	3	2	0	0	0	0	0	0	0	0	0	0	0	0	0
10	0	0	0	0	0	1	3	2	1	0	0	0	0	1	1	0	0	0	0	0	0	0	0
11	0	0	0	0	1	1	2	4	1	1	1	0	1	0	1	1	1	1	3	2	0	0	0
12	0	0	0	0	0	3	1	6	3	0	1	0	1	1	0	1	1	4	1	4	5	1	1
13	0	0	1	1	2	0	1	7	4	0	0	0	0	0	1	3	1	0	1	1	0	2	
14	0	0	0	1	2	3	5	2	1	0	0	0	0	0	1	2	3	0	5	7	2	3	
15	0	0	1	1	5	6	2	5	0	0	0	0	0	0	0	4	1	1	1	1	1	1	
16	0	0	1	1	2	1	3	0	0	0	0	0	0	0	0	6	5	4	5	3	5	2	
17	0	0	1	1	1	5	4	1	0	0	0	0	0	0	0	1	2	7	3	1	1	2	
18	0	0	0	0	2	6	3	3	0	0	0	0	0	0	0	1	3	3	2	1	1	1	
19	0	0	0	0	3	1	5	3	1	0	0	0	0	0	0	1	0	2	0	1	1	1	
20	0	0	0	0	1	2	2	2	2	1	0	0	0	3	0	1	2	3	1	1	0	0	
21	0	0	0	0	0	2	0	0	3	2	1	0	0	0	0	1	1	1	0	0	0	0	
22	0	0	0	0	0	1	0	2	2	1	1	0	1	1	0	1	2	0	0	1	0	0	
23	0	0	0	0	0	0	0	0	0	0	0	0	1	1	1	1	2	0	0	0	0	0	
24	0	0	0	0	0	0	0	0	0	0	0	0	0	0	1	1	0	0	0	0	0	0	
25	0	0	0	0	0	0	0	0	0	0	0	0	0	0	0	0	0	0	0	0	0	0	
26	0	0	0	0	0	0	0	0	0	0	0	0	0	0	0	0	0	0	0	0	0	0	

	0	1	2	3	4	5	6	7	8	9	10	11	12	13	14	15	16	17	18	19	20	21	22
1	19	18	17	17	17	16	16	16	15	15	15	15	15	15	15	16	16	16	17	17	17	18	
2	18	17	17	16	16	15	15	15	14	14	14	14	14	14	14	15	15	15	16	16	16	17	
3	17	16	16	15	15	14	14	14	13	13	13	13	13	13	13	14	14	14	15	15	15	16	
4	16	16	15	14	14	13	13	13	12	12	12	12	12	12	12	13	13	13	14	14	14	15	
5	16	15	14	14	13	13	12	12	11	11	11	11	11	11	11	12	12	13	13	14	14	15	
6	15	14	13	13	12	12	11	11	10	10	10	10	10	10	10	11	11	12	12	13	13	14	
7	14	13	13	12	11	11	10	10	9	9	9	9	9	9	9	10	10	11	11	12	13	13	
8	14	13	12	11	11	10	9	9	9	8	8	8	8	8	9	9	9	10	11	11	12	13	
9	13	12	11	11	10	9	9	8	8	7	7	7	7	7	8	8	9	9	10	11	11	12	
10	13	12	11	10	9	8	8	7	7	6	6	6	6	6	7	7	8	8	9	10	11	12	
11	12	11	10	9	9	8	7	6	6	5	5	5	5	5	6	6	7	8	9	9	10	11	
12	12	11	10	9	8	7	6	6	5	4	4	4	4	4	5	6	6	7	8	9	10	11	
13	11	10	9	9	8	7	6	5	4	4	3	3	3	4	4	5	6	7	8	9	9	10	
14	11	10	9	8	7	6	5	4	4	3	2	2	2	3	4	4	5	6	7	8	9	10	
15	11	10	9	8	7	6	5	4	3	2	1	1	1	2	3	4	5	6	7	8	9	10	
16	11	10	9	8	7	6	5	4	3	2	1	0	1	2	3	4	5	6	7	8	9	10	
17	11	10	9	8	7	6	5	4	3	2	1	1	1	2	3	4	5	6	7	8	9	10	
18	11	10	9	8	7	6	5	4	4	3	2	2	2	3	4	4	5	6	7	8	9	10	
19	11	10	9	9	8	7	6	5	4	4	3	3	3	4	4	5	6	7	8	9	9	10	
20	12	11	10	9	8	7	6	6	5	4	4	4	4	4	5	6	6	7	8	9	10	11	
21	12	11	10	9	9	8	7	6	6	5	5	5	5	5	6	6	7	8	9	9	10	11	
22	13	12	11	10	9	8	8	7	7	6	6	6	6	6	7	7	8	8	9	10	11	12	
23	13	12	11	11	10	9	9	8	8	7	7	7	7	7	8	8	9	9	10	11	11	12	
24	14	13	12	11	11	10	9	9	9	8	8	8	8	8	9	9	9	10	11	11	12	13	
25	14	13	13	12	11	11	10	10	9	9	9	9	9	9	9	10	10	11	11	12	13	13	
26	15	14	13	13	12	12	11	11	10	10	10	10	10	10	10	11	11	12	12	13	13	14	

Figure 7. Pressure distribution of lateral 8 mm beveled defect with pressures (above), and with radius from center to peak (below). (Note: While integer values are displayed for radius in the image, data were not rounded to the integer for analysis.)

Pressure distribution was characterized by analyzing graphs of the pressure over the radius from the center of pressure. Generally, these charts displayed lower pressure values near the defect center, a steep increase at the edge of the defect, a more gradual raise to a peak, a gradual drop-off, and then, a steep drop-off far from the center. This finding agreed with the author's assumption that a circumferential rim of peak pressures would develop at a distance from the defect center.

For each test the peak pressure and location were chosen based on a normalized curve created to outline the general distribution of pressures over the condylar area. To create this curve, peak data were first identified using a skyline approach. This approach consisted of charting peak pressures at each radius from smallest to largest radii on the horizontal axis with corresponding pressure on the vertical axis. Pressures were then normalized with a center-weighted 5-point moving average over the complete range of radii. Creation of this curve greatly helped in removing outliers from each data set. Peak pressure and location were taken from this normalized curve and recorded for analysis.

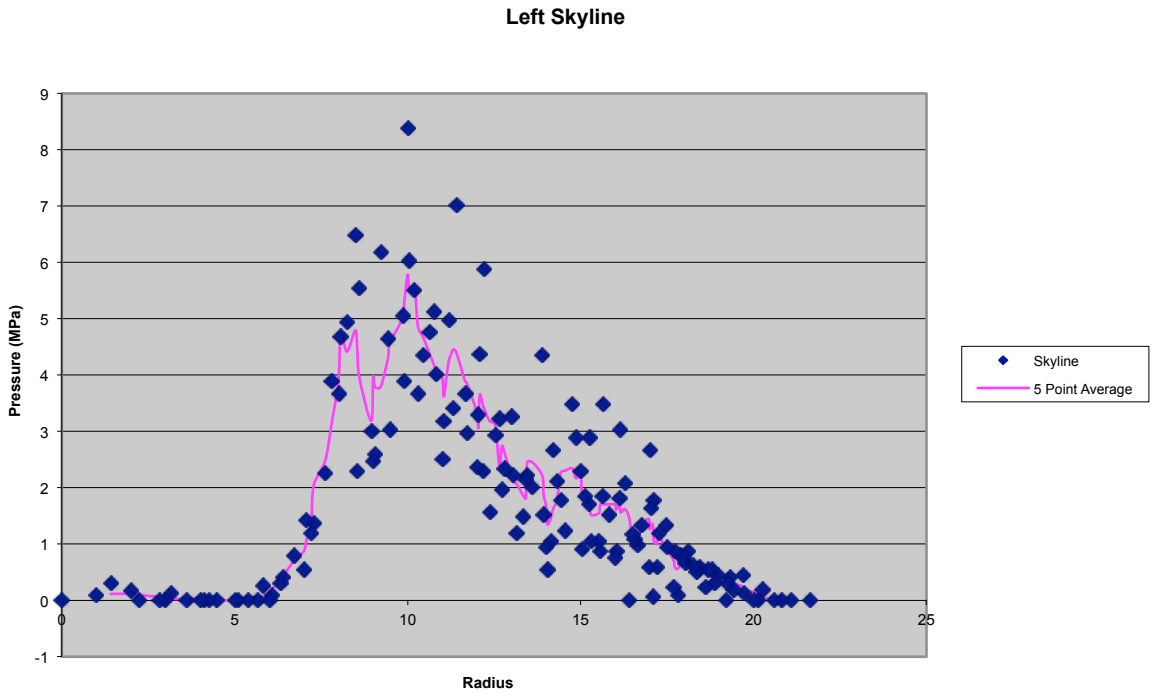

Figure 8. Knee with a 12 mm defect showing skyline and average line, with outliers far from average line.

Statistical tests were used to determine if side (left or right), condyle (medial or lateral), defect type (well-shouldered or beveled), and defect diameter (6 mm to 20 mm) have a significant effect on radius from center to peak. All of the aforementioned factors were included in a four-factor interaction model conceptualized as a randomized complete block design (RCBD) with the specimen as the block. In this initial fitted model, the highest order interaction (i.e. the last term) was tested for statistical significance. This process was repeated iteratively until the simplest model was obtained.

Post-hoc comparisons were performed on this simplest model using a Bonferroni Correction. For each of these models, residual analysis was performed to assess the goodness of fit for each of the fitted models compared to the data, including the assumptions on which the models are based. Continuous data were summarized using mean ± standard deviation, minimum, median and maximum. P-values less than an alpha of 0.05 (Probability of Type I Error) were considered statistically significant. Statistical

analysis was performed using The SAS System for Windows version 9.2 (SAS Institute Inc., Cary, NC).

RESULTS

Upon analysis, it was determined that a peak pressure value and location could be found from the collected data. Each variable of the test (right or left knee, medial or lateral compartment, beveled or well-shouldered defect, and defect diameter) produced a unique pressure profile with a specific location for peak pressure. As described previously this location was used to compare peak stresses based on a theoretical center of defect. This peak pressure and location allows each test variable to be compared in an objective manner. Test data were organized by each of the aforementioned variables into different comparative groups. Each group was scrutinized to determine relationship between the specified variable and the distance from center to peak pressure.

It was observed by the researchers that the 18 mm and 20 mm defects generally came close to and/or breached the borders of the articular cartilage surface that covers the femoral condyle. This observation led to many questions as to the accuracy and usefulness of data obtained from these defect sizes. Also, upon analysis, data for 18 mm and 20 mm defect sizes was found to be significantly skewed from patterns established in the smaller sizes. This finding, in conjunction with the recommendation of multiple orthopaedic surgeons that these sizes were larger than normally seen *in vivo*, led to the decision to remove this data from the results.

For all 6 mm defects, pressure distribution showed a majority of pressure being carried by the meniscus. This was evident in the pressure distribution mappings where the defect rim was hard to distinguish from the surrounding areas of contact pressures. It was assumed here that because of the defect placement and the geometry of the meniscus that at this point the meniscus is carrying a majority of the load. Because of this finding,

there was not a significant rim of peak pressure around the defects and pressure distributions were not significantly altered from the pre-defect state. This phenomenon also carried through to the 8 mm well-shouldered defect in both the medial and lateral condyles. Figures 9 and 10 show two examples of pressure distributions displaying these characteristics.

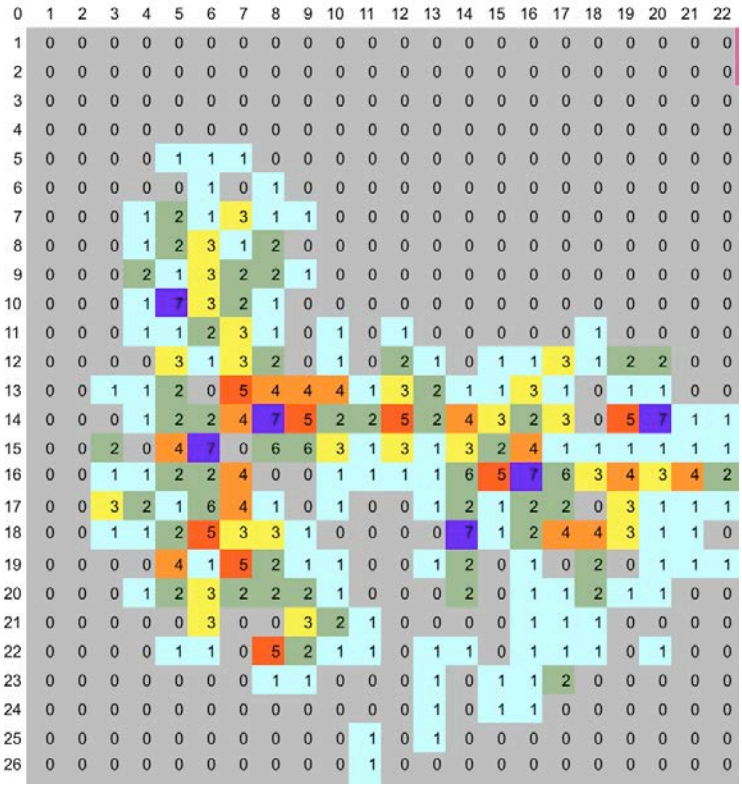

Figure 9. Pressure distribution of 6 mm well-shouldered defect in the lateral compartment of specimen S070521R.

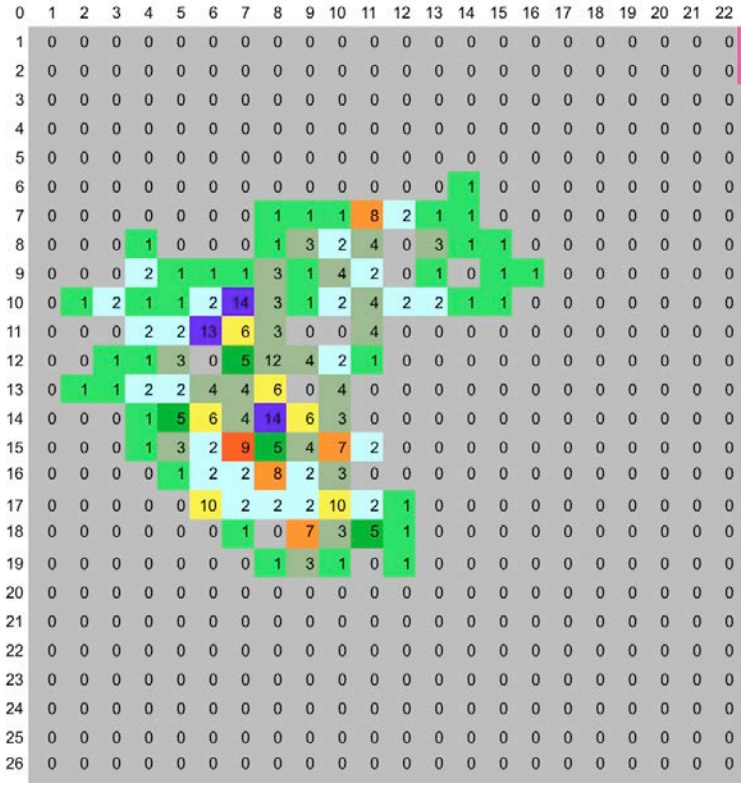

Figure 10. Pressure distribution of 8 mm well-shouldered defect in the medial compartment of specimen S070619L.

In both condyles the 8 mm beveled defects along with the 10, 12, 14 and 16 mm beveled and well-shouldered defects displayed a notable defect rim. It was assumed that as the defect grew in size it gradually came into contact with the meniscus and caused pressures to be redistributed around the defect. This disruption in pressure distribution from the standard pattern was an important finding.

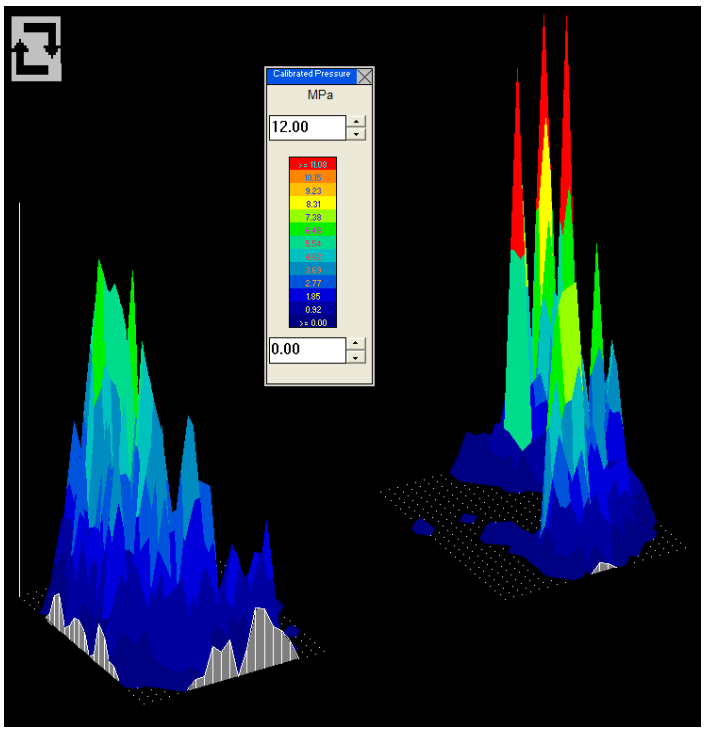

Figure 11. 12 mm beveled defect pressure distribution (isometric view).

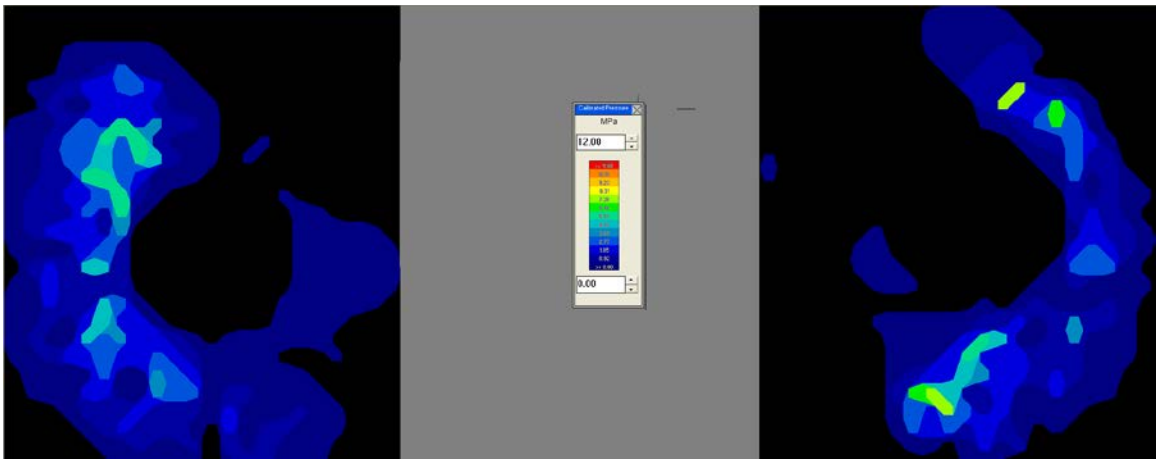

Figure 12. 12 mm beveled defect pressure distribution (top view).

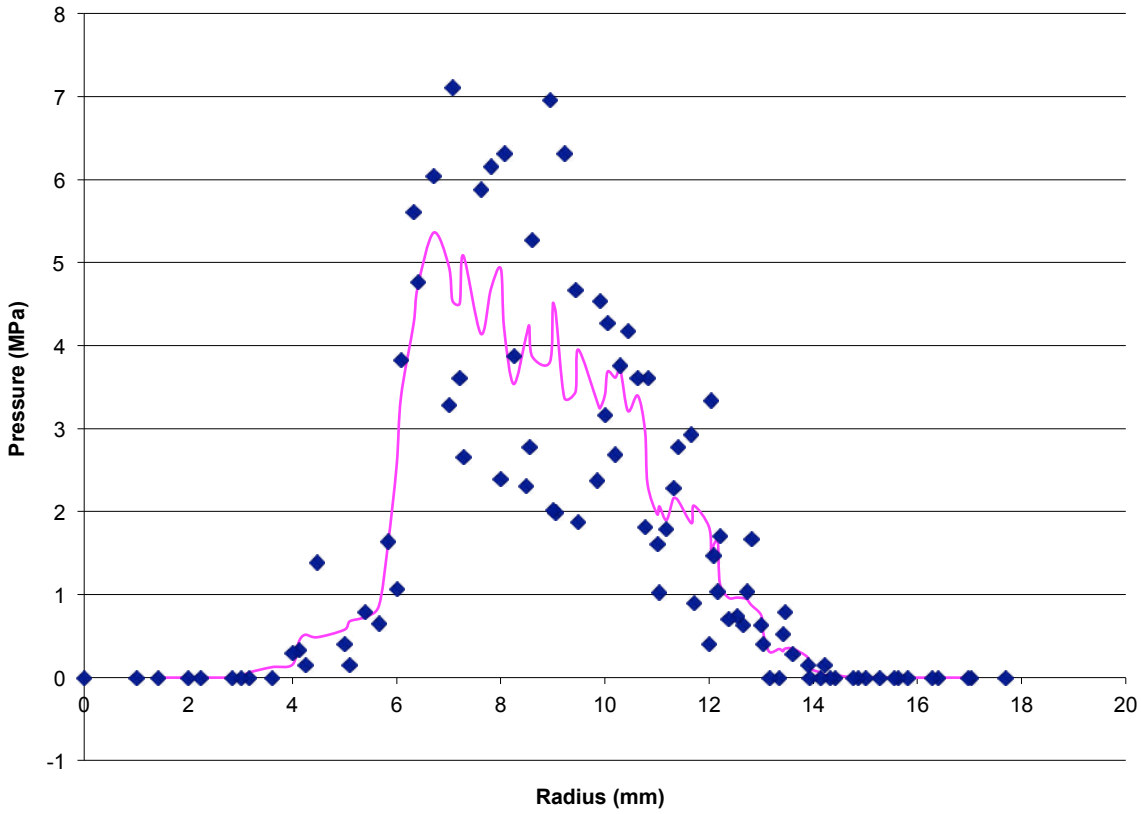

Figure 13. Pressures around a 12 mm beveled defect in the lateral compartment of specimen S070323R, organized radially from center of defect. Note: Blue diamonds indicate raw pressure values; the pink line shows pressure values after 5-point averaging.

An example of disruption in articular pressure distribution is shown in the above figures. Figures 11 and 12 show two different graphical representations of the pressure distributions in a right knee with a 12 mm defect. From these we can observe a very obvious defect center and defect rim. Also, a rim of peak pressures can be seen, but this phenomenon is not as obvious as the center and defect diameter. Because of this, graphs were created correlating pressure value at each sensel with its distance from the center of the defect. This radial distribution (shown in Figure 13) shows a definitive area of peaks in the 7 mm to 11 mm range with a peak at 7 mm. The change in distribution can be seen when compared with the same specimen with a 6 mm defect (below). The 6 mm defect

does not show a defined center or rim of peak pressures like that seen in the larger defects. Instead, pressures are distributed much more widely over the condylar surface.

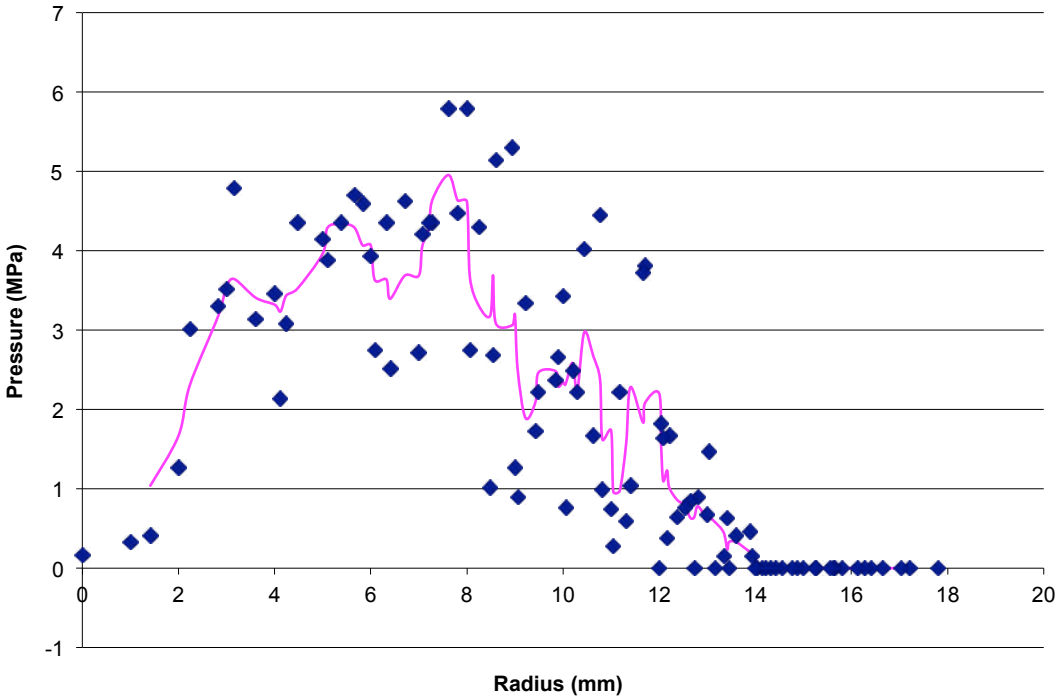

Figure 14. Pressures around a 6 mm well-shouldered defect in the lateral compartment of specimen S070323R.

Based on these trends peak pressure and location of peak pressure (radius from defect center) for each test variable were readily identifiable. Table 1 lists the determined radius from defect center to peak pressure and the corresponding peak pressure for each defect size, averaged over the sample of 10 specimens tested. Individual results for each specimen are included in the Appendix.

	Radius to Peak (mm)		Peak Pressure (MPa)	
Defect	Lateral	Medial	Lateral	Medial
6 mm	7.7	8.2	4.44	6.23
6 mm (B)	7.9	9.0	4.54	6.10
8 mm	8.0	9.5	4.69	6.34
8 mm (B)	9.4	10.8	4.64	6.26
10 mm	9.2	10.1	4.70	6.44
10 mm (B)	8.9	10.9	4.81	5.97
12 mm	9.7	11.3	5.03	6.14
12 mm (B)	9.7	10.7	4.96	6.83
14 mm	9.6	10.6	5.23	6.31
14 mm (B)	10.3	10.4	5.27	7.13
16 mm	10.7	10.2	5.01	6.78
16 mm (B)	11.3	10.7	4.98	7.30

Table 1. Averaged radius from center to peak and corresponding pressure for each defect size. Note: (B) indicates a beveled defect.

Important findings from this data set were first and foremost that this study validates the previous study conducted by Guettler et al. In this study it was found that on the left side radius from center to peak increases with defect diameter. The increase from 6 mm to 16 mm defects is 3.8 mm ($p = 0.0029$). Also, it was found that the radius from center to peak increases with defect diameter on the right side. The change in radius over the range of specimens 6 mm to 16 mm is 3.3 mm ($p = 0.0173$). This includes both well-shouldered and beveled defects, in the medial and lateral compartments. These findings agree with the previous study insomuch as a statistically significant rim of peak pressure concentrations was found and that this rim of peak pressure concentrations follows the rim of the defect. As this study did not aim to reassess the minimum defect size at which to operate, no statistical tests were run to test this. However, this phenomenon can be seen observed in the data from this study.

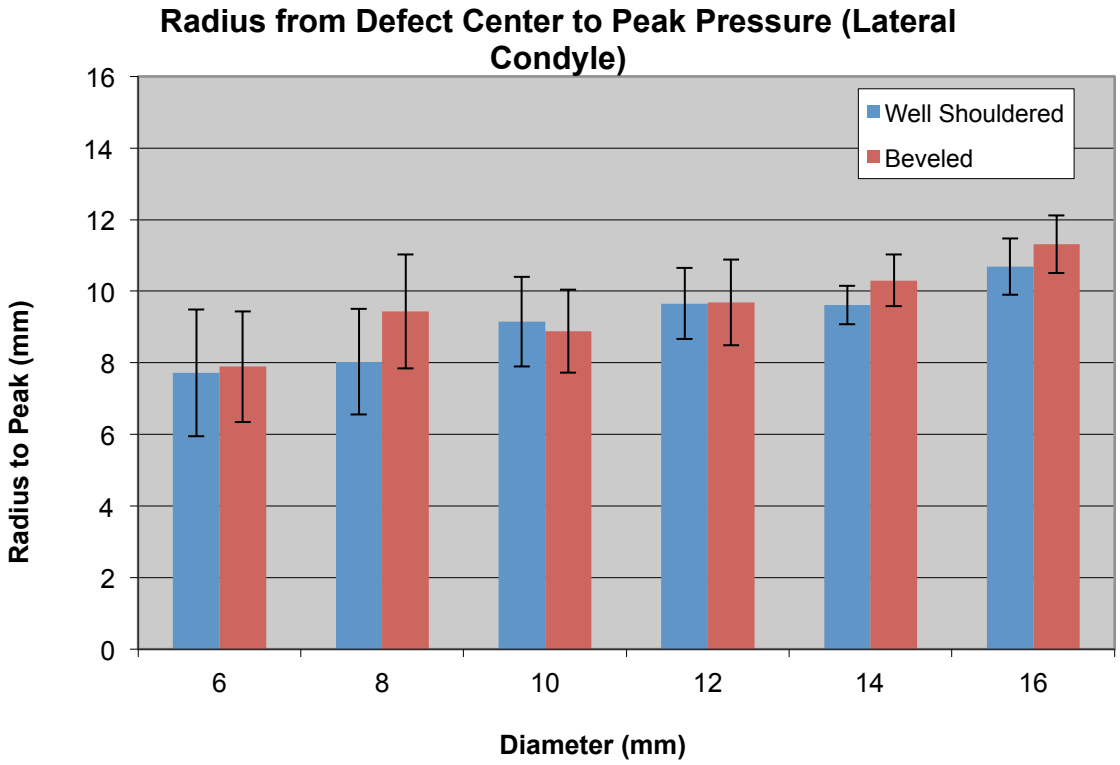

Figure 15. Comparison of radius from center to peak pressure of well-shouldered and beveled defects in the lateral condyle.

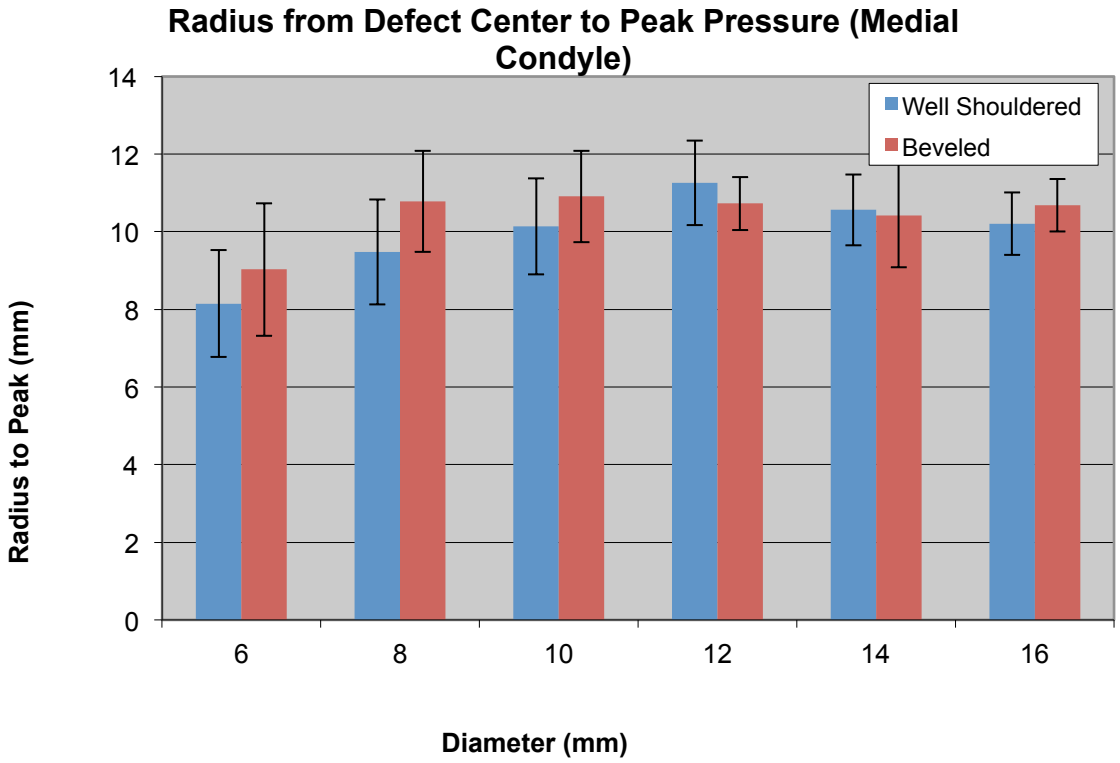

Figure 16. Comparison of radius from center to peak pressure of well-shouldered and beveled defects in the medial condyle.

Average radius from center to peak was found to be higher for beveled defects (10.0 ± 0.5 mm) than for well-shouldered defects (9.6 ± 0.6 mm) over the range of defects tested, although this was not found to be statistically significant ($p > 0.05$). Also, the average center to peak pressure distance was found to be 0.4 ± 0.3 mm higher for beveled defects than well-shouldered defects in the lateral condyle. In the medial condyle it was found to be 0.5 ± 0.3 mm higher for beveled defects than well-shouldered defects. These results also showed no statistical significance ($p > 0.05$). Figures 15 and 16 show graphical representations of the comparison between well-shouldered and beveled defects.

Average radius from center to peak of the medial condyle (10.2 ± 0.5 mm) was higher than that of the lateral condyle (9.4 ± 0.6 mm). Pressures were consistently higher in the medial condyle (6.5 ± 0.2 MPa) than in the lateral condyle (4.9 ± 0.1 MPa). Peak pressures did not show any significant increase as defect diameter increased ($p > 0.05$).

Additionally, analysis was conducted by subtracting the defect radius from the center to peak radius recorded for each defect. For this operation the outer diameter of the defects were used, for example an 8 mm well-shouldered defect has an 8 mm diameter, whereas an 8 mm beveled defect has a 10 mm diameter. These results showed a decreasing radius from the edge of the defect to the peak pressure as defect diameter increased. The average decrease in the lateral condyle was 2.4 ± 1.5 mm and 3.5 ± 1.7 mm in the medial condyle. These decreases are over the full range of defect sizes. Figures 17 and 18 show a graphical representation of this trend. This trend was not found to show statistical significance.

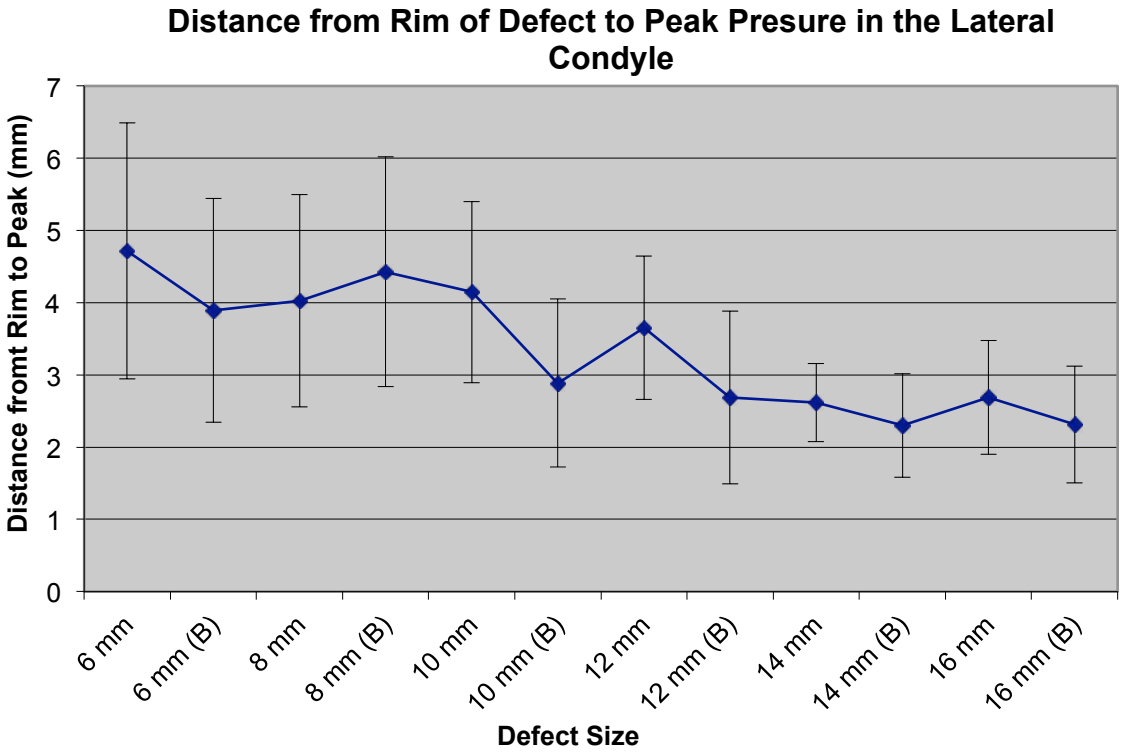

Figure 17. Distance from the rim of the defect to the peak pressure for the lateral condyle. Note: (B) indicates a beveled defect.

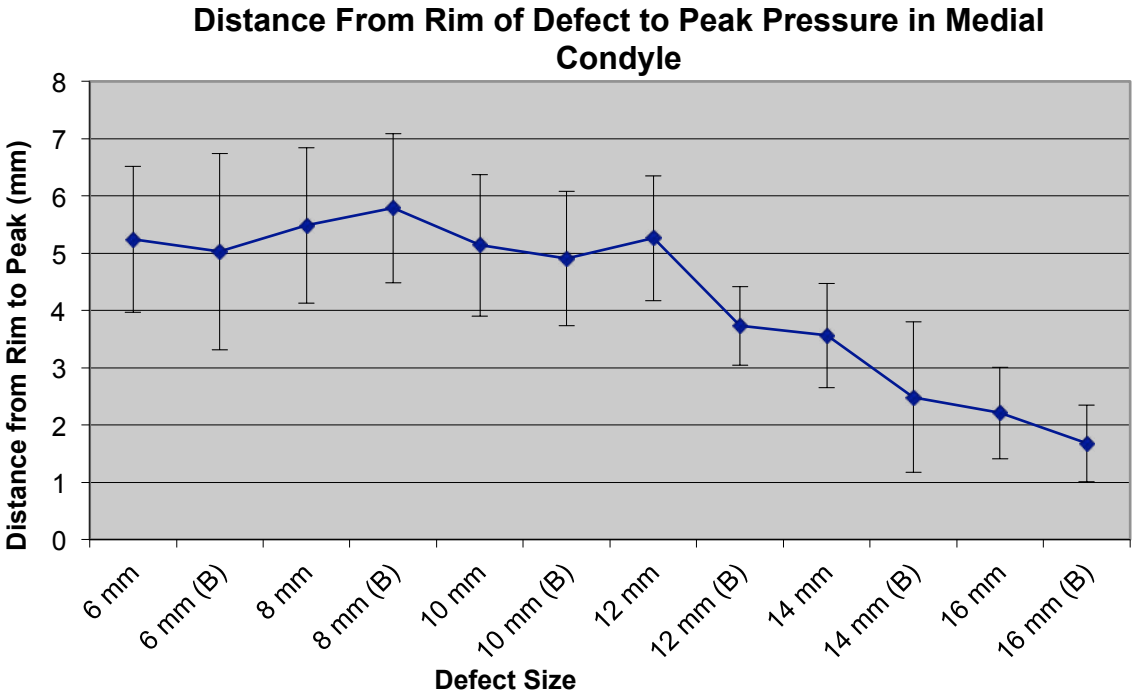

Figure 18. Distance from the rim of the defect to the peak pressure for the medial condyle. Note: (B) indicates a beveled defect.

Please note that listed uncertainty of mean values in the above figures is represented by one standard deviation.

DISCUSSION

Articular cartilage is known to possess limited regenerative potential[3,12,14]. Damaged cartilage can cause pain, joint dysfunction and effusions[4]. Osteochondral defect degeneration is multifactorial and comorbidities such as cruciate deficiency, meniscal damage, limb malalignment, and obesity should be considered[6] when evaluating outcomes. Long-term follow-up studies have shown existing cartilage defects have a tendency towards further degeneration[11,16,23]. Also, The aim of this study is to further quantify causality in the progressive degeneration of damaged articular cartilage.

This study paired with other previously discussed studies shows that as an osteochondral defect grows, pressure onset by physiological loading will redistribute further away from the center of the defect. Consideration of these studies together cement both the fact that when assessing articular cartilage damage, defect size is an important criteria to evaluate, and that defects of diameter 10 mm or greater will show defect rim stress concentrations not seen in healthy joints. This finding is contrary to the commonly quoted defect size of 16 mm (2 cm^2) at which surgical intervention is recommended[6,17,18].

Further, this study sought to investigate the influence of defects of differing morphology on peak rim stress distribution. As can be seen from the results, beveled defects show a broader redistribution of peak pressures than their well-shouldered counterparts. Unfortunately, this phenomenon is shown in the comparison of means and did not achieve statistical significance. It is believed that the reasons for the lack of statistical significance are two-fold. Firstly, the physiological attributes of specimens were found to differ significantly from one to the next. This shows itself insomuch as the

range of center to peak distances was large over the whole sample set, creating a large margin of error. For example, specimen S070323R has center to peak radii ranging from 9.6 mm to 12.5 mm in the lateral compartment, whereas these radii range from 6.3 mm to 9.2 mm in the lateral compartment for specimen S070619L. A correction factor was considered for these data, but not implemented as this was not used on previous studies and would significantly alter the data. Secondly, the sample size was small. A multi-fold increase in sample size would likely produce more significance in the differences between beveled and well-shouldered defect center to rim of peak pressures radii. However this undertaking was well beyond our scope and further study was not considered within the scope of this biomechanical study.

The 10 mm threshold effect described previously can be seen specifically and graphically in the data for rim of defect to peak pressure. These data portray a rim of peak pressures moving with defect size until it reaches 10 mm. At this point the rim of peak pressures moves away from the rim of the defect at larger distance increments than those of the defect size increases.

This study itself created many questions. Osteochondral defect shapes used were based on clinical experience and anecdotal evidence only, as no significant empirical research was found describing typical osteochondral defect geometries. The articular cartilage was assumed to deform in a manner that would not affect the location or geometry of the defect. However, as the actual deformation was not observed or modeled, its effects may prove more relevant than assumed. In some instances pressure readings were found within the preloaded diameter of the defect, this phenomenon was not extensively evaluated, but data suggests the possibility of unforeseen deformation of the

defect walls. Further study of this phenomenon may lead to a better understanding of the locations of rims of peak pressures observed in this study.

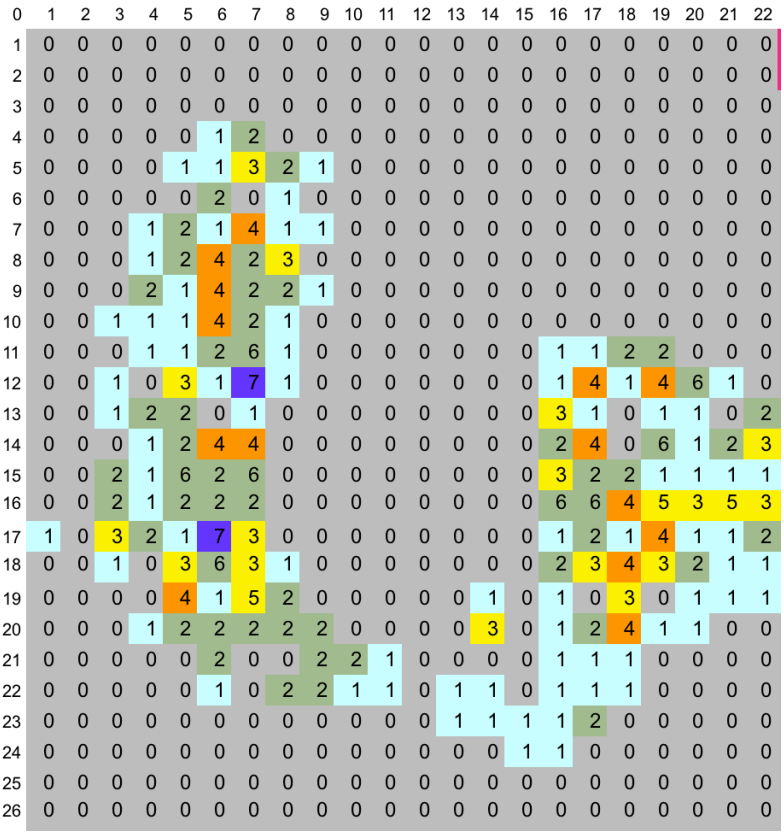

Figure 19. 10 mm well-shouldered pressure reading data showing pressures starting as close as 3 sensels (approximately 4mm) from the defect center.

Simonian et al. completed a similar study to determine contact pressures found at typical osteochondral autograft donor sites used for autologous osteochondral transplantation[20]. These donor sites were located around the femoral intercondylar notch and the periphery of the lateral femur at the patellofemoral joint. Findings of this study showed that all sites tested are articulating and demonstrated significant contact pressure over a range of 0° to 110° flexion. The current study found peak pressures being redistributed outward as defect size grew. In the larger defects, pressure distributions pushed to the edge of the condyle reaching these locations tested by Simonian et al. As

this study tested 30° of flexion, testing at differing positions of knee flexion through a normal physiological range of 0° to 110°[7] may present a more complete understanding of contact stresses seen during daily activity. These different positions have the possibility of showing contact pressure distributions significantly altered beyond what was seen in this study.

This study has other limitations not discussed above including: (1) this is a simplistic biomechanical model that only approximates what occurs in the natural dynamic state of the knee; (2) these defects were loaded in a concentric manner under a single load level whereas the human knee is loaded in a more complex eccentric manner over a range of loads under normal physiologic conditions; (3) the study did not take into account the capacity for repair since a cadaveric model was used instead of a living knee; (4) the loading model did not replicate typical impact-loading seen in a living system; (5) this study did not address the effect of cumulative stress on cartilage adjacent to the defects; (6) the median age of specimens tested was 65 years, although each knee was inspected for articular and meniscal damage, this could have affected our results if unseen damage was present; and (7) only one angle of beveled lesion was investigated, in reality multiple wall angles would be present, varying from patient to patient. This wall angle could have biomechanical implications to the response of the tested lesions.

In this study the authors hypothesize that load redistribution onto healthy cartilage adjacent to osteochondral defects is the cause of degenerative changes in those areas. Jackson et al. demonstrated that increased rim stress concentrations lead to degenerative changes in adult goats[13]. The authors postulated that redistribution of loads may have been a cause for the degeneration. Wei et al. in a rabbit study showed that cartilage

adjacent to a defect exhibits degeneration, especially in younger specimens[22]. Based on these studies it is easy to assume that load redistribution is the cause for degenerative changes in adjacent cartilage. However, this phenomenon cannot be ascertained, as there is no empirical evidence proving this link. It was shown in our study that peak stresses do not increase significantly as defect size increases. It was also shown that although peak stresses do not change, the concentration of peak stresses moves from an even distribution to a narrower rim as the defects increase in size above 10 mm. Although these findings may not prove that pressure redistribution is linked to degeneration of adjacent cartilage, they are another step towards establishing a link between the two.

CONCLUSIONS

Articular cartilage is extraordinary insomuch as its mechanical properties give it the ability to resist cyclic loading for a lifetime. However, its limited capacity to regenerate makes it prone to degeneration upon injury. Because of this, surgeons are left with the question of what measureable indications constitute a cartilage injury in need of surgical intervention.

Seeking to answer this question, this study was able to reinforce previous work by Brown et al. and Guettler et al. that indicate a threshold size for osteochondral defects, above which contact pressures are redistributed from the meniscal loading area to the surrounding cartilage. Also this study was able to demonstrate that defects with irregular or beveled borders tend to act more like larger non-beveled defects. However, this phenomenon was not found to be statistically significant. There are many possible explanations for this. It is believed by the author that the minute differences in pressure distributions found between the two defect types coupled with the substantial naturally occurring anatomical differences between specimens led to variability in outcomes our statistical model was unable to overcome. Also, the relatively small sample size likely affected this outcome.

Although statistical significance was not proven, the author still recommends that physicians assessing whether or not surgical intervention is necessary should consider the diameter of the outermost border of the osteochondral defect when comparing to the 10 mm threshold size recommended by Guettler et al.[10] In addition, as many studies have linked articular cartilage defects to degeneration of the surrounding cartilage, it seems

prudent to err on the side of caution and consider defects based on their outer diameter when assessing need for surgical intervention.

APPENDIX

COMPLETE LIST OF EXPERIMENTAL DATA

Specimen	Radius to Peak(mm)		Peak Pressure (MPa)	
S070323L	Lateral	Medial	Lateral	Medial
6mm	16.5	9.2	3.71	6.15
6 mm (B)	14.9	9.2	3.27	5.66
8mm	15.4	12.0	4.87	6.13
8 mm (B)	14.4	12.9	5.53	5.94
10mm	15.4	11.4	4.88	5.97
10 mm (B)	14.4	11.4	5.59	5.99
12mm	14.0	11.4	6.04	5.20
12 mm (B)	16.2	10.8	4.78	5.65
14mm	10.2	12.0	5.88	5.62
14 mm (B)	13.2	10.8	5.94	5.51
16mm	10.5	12.0	4.25	6.56
16 mm (B)	12.9	10.8	3.34	6.35

Specimen	Radius to Peak(mm)		Peak Pressure (MPa)	
S070323R	Lateral	Medial	Lateral	Medial
6mm	9.7	10.8	4.96	6.08
6 mm (B)	9.7	10.8	4.91	5.41
8mm	9.7	12.0	5.01	6.18
8 mm (B)	10.8	12.9	4.84	5.64
10mm	8.9	12.0	4.78	6.38
10 mm (B)	6.8	10.2	5.34	5.20
12mm	10.5	10.8	5.41	5.96
12 mm (B)	8.5	9.9	5.36	7.36
14mm	9.2	8.5	5.81	6.60
14 mm (B)	10.8	9.2	5.64	7.58
16mm	10.5	8.5	5.88	5.24
16 mm (B)	12.5	9.2	5.77	9.45

S070399L	Radius to Peak(mm)		Peak Pressure (MPa)	
S070399L	Lateral	Medial	Lateral	Medial
6mm	8.5	8.9	4.38	7.37
6 mm (B)	5.4	8.5	5.06	6.29
8mm	8.1	9.2	5.20	6.68
8 mm (B)	14.2	11.4	4.69	7.34
10mm	9.9	12.0	5.37	7.74
10 mm (B)	10.5	14.5	4.62	5.60
12mm	9.9	14.5	5.39	7.36
12 mm (B)	8.5	13.5	4.51	7.24
14mm	9.2	13.7	5.89	5.87
14 mm (B)	11.4	17.3	5.10	6.20
16mm	13.2	13.5	4.41	8.34
16 mm (B)	12.7	13.5	5.66	9.80

Specimen	Radius to Peak(mm)		Peak Pressure (MPa)	
S070619L	Lateral	Medial	Lateral	Medial
6mm	6.3	2.5	3.94	8.98
6 mm (B)	4.6	6.3	3.94	7.78
8mm	5.4	8.5	4.18	7.85
8 mm (B)	6.8	9.0	4.06	8.28
10mm	8.5	8.0	3.97	8.72
10 mm (B)	6.5	10.2	4.31	7.09
12mm	8.0	9.2	4.88	7.35
12 mm (B)	9.0	10.8	5.00	6.57
14mm	9.2	8.0	5.49	6.68
14 mm (B)	9.2	8.88	6.06	6.81
16mm	9.2	9.23	5.82	8.19
16 mm (B)	9.2	11.35	5.58	8.19

Specimen	Radius to Peak(mm)		Peak Pressure (MPa)	
S070619R	Lateral	Medial	Lateral	Medial
6mm	3.8	6.5	3.95	5.69
6 mm (B)	5.4	6.3	3.77	7.54
8mm	6.3	5.7	4.55	6.76
8 mm (B)	5.4	7.7	3.33	6.47
10mm	10.2	7.4	4.88	5.94
10 mm (B)	7.2	8.0	4.45	7.26
12mm	11.5	8.1	3.88	5.70
12 mm (B)	9.0	9.0	4.08	7.01
14mm	9.0	9.2	4.85	5.40
14 mm (B)	9.9	8.5	4.37	9.89
16mm	13.1	8.5	3.98	5.30
16 mm (B)	10.2	9.2	4.37	5.64

Specimen	Radius to Peak(mm)		Peak Pressure (MPa)	
S070399R	Lateral	Medial	Lateral	Medial
6mm	4.6	11.4	4.49	5.67
6 mm (B)	8.9	16.7	4.95	6.23
8mm	6.8	10.8	4.91	5.62
8 mm (B)	8.9	12.9	5.29	5.78
10mm	6.8	10.8	5.20	5.62
10 mm (B)	8.0	14.5	4.73	4.90
12mm	6.8	10.8	5.46	5.13
12 mm (B)	8.0	12.0	6.54	6.83
14mm	8.0	12.0	5.31	6.31
14 mm (B)	9.2	7.7	5.42	6.44
16mm	9.2	9.2	5.17	7.29
16 mm (B)	9.2	10.8	5.47	6.70

Specimen	Radius to Peak(mm)		Peak Pressure (MPa)	
S070521L	Lateral	Medial	Lateral	Medial
6mm	6.5	10.5	4.73	5.69
6 mm (B)	5.7	6.8	4.72	6.85
8mm	6.5	8.5	4.62	5.78
8 mm (B)	5.7	11.4	4.39	5.89
10mm	8.0	6.5	3.84	7.49
10 mm (B)	8.9	8.9	4.08	6.48
12mm	9.0	14.0	5.24	7.16
12 mm (B)	10.2	10.2	5.77	7.88
14mm	11.4	9.2	5.07	7.16
14 mm (B)	11.5	10.8	5.25	9.20
16mm	12.0	10.2	4.82	8.30
16 mm (B)	14.0	9.2	4.87	7.17

Specimen	Radius to Peak(mm)		Peak Pressure (MPa)	
S070521R	Lateral	Medial	Lateral	Medial
6mm	6.3	5.2	6.19	4.12
6 mm (B)	6.3	5.1	6.21	5.25
8mm	6.3	5.7	5.65	7.14
8 mm (B)	7.7	6.5	5.49	6.48
10mm	6.5	7.6	5.94	8.46
10 mm (B)	8.5	8.1	5.99	6.55
12mm	8.5	8.9	5.26	5.86
12 mm (B)	10.2	9.0	4.92	7.22
14mm	8.9	11.4	5.45	7.26
14 mm (B)	10.2	10.2	5.15	7.85
16mm	9.2	10.9	6.70	6.60
16 mm (B)	10.8	11.4	5.96	7.46

Specimen	Radius to Peak(mm)		Peak Pressure (MPa)	
S070599L	Lateral	Medial	Lateral	Medial
6mm	6.8	8.9	4.70	5.63
6 mm (B)	9.0	12.0	4.94	5.13
8mm	6.5	14.0	4.36	5.26
8 mm (B)	10.8	14.2	5.07	4.75
10mm	9.2	13.1	5.16	4.72
10 mm (B)	10.2	12.6	5.15	5.52
12mm	9.2	11.5	4.84	6.35
12 mm (B)	9.2	11.5	4.73	6.84
14mm	11.4	11.5	4.54	6.20
14 mm (B)	8.5	11.7	5.28	7.24
16mm	9.2	10.8	4.95	7.05
16 mm (B)	10.8	9.9	4.44	5.97

Specimen	Radius to Peak(mm)		Peak Pressure (MPa)	
S070599R	Lateral	Medial	Lateral	Medial
6mm	8.1	7.6	3.34	6.95
6 mm (B)	9.2	8.5	3.68	4.85
8mm	9.2	8.5	3.58	6.03
8 mm (B)	9.7	8.9	3.73	6.02
10mm	8.0	12.6	3.67	5.51
10 mm (B)	8.0	10.8	3.79	5.12
12mm	9.2	13.5	3.91	5.35
12 mm (B)	8.1	10.8	3.88	5.70
14mm	9.7	10.2	4.03	6.04
14 mm (B)	9.2	9.2	4.45	4.57
16mm	10.8	9.2	4.11	4.93
16 mm (B)	10.8	11.5	4.32	6.29

REFERENCES

1. Akeson WH. Articular Cartilage and its Exacting Characteristics: The Benchmark for All Attempts to Achieve Articular Cartilage Regeneration or Repair. *Daniel's Knee Injuries.* 2003:113-125.

2. Brown TD, Pope DF, Hale JE, Buckwalter JA, Brand RA. Effects of osteochondral defect size on cartilage contact stress. *J Orthop Res.* Jul 1991;9(4):559-567.

3. Buckwalter JA, Rosenberg LC, Hunziker EB. Articular Cartilage: composition, structure, response to injury, and methods of facilitating repair. In: Ewing JW, ed. . *Articular Cartilage and Knee Joint Function: Basic Science and Arthroscopy.* 1990:19-56.

4. Buckwalter JA. Articular cartilage: Injuries and potential for healing. *Journal of Orthopeadic Sports Physical Therapy.* 1998;28(4):192-202.

5. Chu CR. Cartilage Therapies: Chondrocyte Transplantation, Osteochondral Allografts, and Autografts. *Daniel's Knee Injuries.* 2003:227-237.

6. Cole BJ, Cohen B. Chondral injuries of the knee. *Orthopedic Special Edition.* 2000;6:71-76.

7. Daluga D, Lombardi AV, Jr., Mallory TH, Vaughn BK. Knee manipulation following total knee arthroplasty. Analysis of prognostic variables. *J Arthroplasty.* Jun 1991;6(2):119-128.

8. Flik KR, Verma N, Cole BJ, Bach BR. Articular Cartilage: Structure, Biology, and Function. *Cartilage Repair Strategies.* 2007:1-12.

9. Gray H, Williams PL. *Gray's anatomy*. 37th ed. Edinburgh ; New York: C. Livingstone; 1989.

10. Guettler JH, Demetropoulos CK, Yang KH, Jurist KA. Osteochondral defects in the human knee: influence of defect size on cartilage rim stress and load redistribution to surrounding cartilage. *Am J Sports Med.* Sep 2004;32(6):1451-1458.

11. Hughston JC, Hergenroeder PT, Courtenay BG. Osteochondritis dissecans of the femoral condyles. *Journal of Bone and Joint Surgery of America.* 1984;66:1340-1348.

12. Hunter W. Of the structure and disease of articulating cartilages. *Clinical Orthopaedics.* 1995;317:3-6.

13. Jackson DW, Lalor PA, Aberman HM, Simon TM. Spontaneous repair of full-thickness defects of articular cartilage in a goat model. A preliminary study. *J Bone Joint Surg Am.* Jan 2001;83-A(1):53-64.

14. Mankin HJ. The response of articular cartilage to mechanical injury. *J Bone Joint Surg Am.* Mar 1982;64(3):460-466.

15. Marx R. Evaluating outcome following cartilage procedures. *Cartilage Repair Strategies.* 2007:13-17.

16. Messner K, Maletius W. The long-term prognosis for sever damage to weight-bearing cartilage in the knee: a 14-year clinical and radiographic follow-up in 28 young athletes. *Acta Orthopaedica Scandinavia.* 1996;67(2):165-168.

17. Minas T, Nehrer S. Current concepts in the treatment of articular cartilage defects. *Orthopedics.* 1997;20(6):525-538.

18. Minas T. The role of cartilage repair techniques, including chondrocyte transplantation, in focal chondral knee damage. *Instructional Course Lectures.* 1999;48:629-643.

19. Mow VC, Holmes MH, Lai WM. Fluid transport and mechanical properties of articular cartilage: a review. *J Biomech.* 1984;17(5):377-394.

20. Simonian PT, Sussmann PS, Wickiewicz TL, Paletta GA, Warren RF. Contact Pressures at Osteochondral Donor Sites in the Knee. *American Journal of Sports Medicine.* 1998;26(4):491-494.

21. Vijayan S, Bentley G, Briggs TWR, et al. Cartilage repair: A review of Stanmore experience in the treatment of osteochondral defects in the knee with various surgical techniques. *Indian Journal of Orthopaedics.* 2010;44(3):238-245.

22. Wei X, Gao J, Messner K. Maturation-dependent repair of untreated osteochondral defects in the rabbit knee joint. *J Biomed Mater Res.* Jan 1997;34(1):63-72.

23. Wolfe F, Lane NE. The longterm outcome of osteoarthritis: rates and predictors of joint space narrowing in symptomatic patients with knee osteoarthritis. *J Rheumatol.* Jan 2002;29(1):139-146.

ABSTRACT

CONTACT PRESSURE PROPERTIES OF OSTEOCHONDRAL DEFECTS OF THE KNEE: THE EFFECT OF NON-VERTICAL WALLS

by

SCOTT ENSMINGER

December 2012

Advisor: Dr. King-Hay Yang

Major: Mechanical Engineering

Degree: Master of Science

Purpose: To examine the relationship between well-shouldered osteochondral defects and defects of different geometries by studying their effects on rim stress concentration and load redistribution in the human knee.

Methods: Ten fresh-frozen cadaveric knees were mounted at 30° of flexion in a materials testing machine. Digital electronic pressure sensors were placed in the medial and lateral compartments of the knee. Dynamic pressure readings were recorded throughout the loading and holding phases as each knee was loaded to 700N and held for 5 seconds. Artificial defects were created in each knee to simulate well-shouldered defects and beveled-defects. Loading was repeated for well-shouldered and beveled osteochondral defects sized 6, 8, 10, 12, 14, 16, 18 and 20 mm.

Results: Stress concentrations around rims of defects were shown to act similarly to a previous study by Guettler et al. As defect size increased, a rim of peak pressures formed on the adjacent cartilage with distance from defect center to rim of peak pressures increasing as defect size increased ($p<0.05$). Average radius from the center to the rim of peak pressure was found to be higher among beveled defects although this was not found

to be statistically significant. Peak pressure values did not increase significantly as defects were enlarged.

Conclusions: Beveled defects were found to affect rim stress concentrations over their well-shouldered counterparts. Although this result was not statistically significant, multiple studies point to a link between osteochondral defects and degeneration of surrounding articular cartilage. Based on this finding, it would be prudent when using a size criterion in assessing severity of an osteochondral defect, to use the outermost border of the defect as a measure of defect size.

AUTOBIOGRAPHICAL STATEMENT

Scott Ensminger is an engineer currently working on industrial projects in China and Russia. He is originally from Waterford, Michigan and attended the University of Michigan for his undergraduate studies in Mechanical Engineering. His interest in the subject of this thesis was spurred by involvement in multiple biomechanical studies while working at the Harold W. Gehring, M.D. Center for Biomechanics and Implant Analysis, part of the research institute at William Beaumont Hospital.